

Revealing the Bonding Nature and Electronic Structure of Early-Transition-Metal Dihydrides

Curran Kalha¹, Laura E. Ratcliff², Giorgio Colombi³, Christoph Schlueter⁴, Bernard Dam³, Andrei Gloskovskii⁴, Tien-Lin Lee⁵, Pardeep K. Thakur⁵, Prajna Bhatt¹, Yujiang Zhu¹, Jürg Osterwalder⁶, Francesco Offi⁷, Giancarlo Panaccione^{8,*} and Anna Regoutz^{1,†}

¹Department of Chemistry, University College London (UCL), 20 Gordon Street, London WC1H 0AJ, United Kingdom

²Centre for Computational Chemistry, School of Chemistry, University of Bristol, Bristol BS8 1TS, United Kingdom

³Materials for Energy Conversion and Storage, Department of Chemical Engineering, Delft University of Technology, Delft NL-2629HZ, The Netherlands


⁴Deutsches Elektronen-Synchrotron (DESY), Notkestraße 85, Hamburg 22607, Germany

⁵Diamond Light Source Ltd., Diamond House, Harwell Science and Innovation Campus, Didcot OX11 0DE, United Kingdom

⁶Physik-Institut, Universität Zürich, Zürich CH-8057, Switzerland

⁷Dipartimento di Scienze, Università di Roma Tre, Rome 00146, Italy

⁸Istituto Officina dei Materiali (IOM)-CNR, Laboratorio TASC, in Area Science Park, S.S.14, Km 163.5, Trieste I-34149, Italy

 (Received 30 May 2023; revised 28 September 2023; accepted 2 November 2023; published 16 January 2024)

Metal hydrides are potential candidates for applications in hydrogen-related technologies, such as energy storage, hydrogen compression, and hydrogen sensing, to name just a few. However, understanding the electronic structure and chemical environment of hydrogen within them remains a key challenge. This work presents a new analytical pathway to explore these aspects in technologically relevant systems using hard x-ray photoelectron spectroscopy (HAXPES) on thin films of two prototypical metal dihydrides: $\text{YH}_{2-\delta}$ and $\text{TiH}_{2-\delta}$. By taking advantage of the tunability of synchrotron radiation, a nondestructive depth profile of the chemical states is obtained using core-level spectra. Combining experimental valence-band (VB) spectra collected at varying photon energies with theoretical insights from density functional theory (DFT) calculations, a description of the bonding nature and the role of *d* versus *sp* contributions to states near the Fermi energy are provided. Moreover, a reliable determination of the enthalpy of formation is proposed by using experimental values of the energy position of metal *s*-band features close to the Fermi energy in the HAXPES VB spectra.

DOI: [10.1103/PRXEnergy.3.013003](https://doi.org/10.1103/PRXEnergy.3.013003)

I. INTRODUCTION

Metal hydrides are studied due to their potential in various energy-related applications, such as energy storage [1–3], hydrogen compression [3], hydrogen separation membranes [4], smart windows [5], and hydrogen sensing [6]. The most successful application is still its use as

an electrode in metal-hydride batteries [2]. Essential features of metal hydrides are the reversibility of hydrogen absorption, the tunable absorption, and a volumetric hydrogen density higher than that of compressed or liquefied hydrogen. In addition, the development of thin-film optical hydrogen sensors relies on the change in optical properties on absorption [5,7,8]. These properties are heavily dictated by their thermodynamic behavior and, by extension, their electronic structure. Therefore, a fundamental understanding of the electron interaction between hydrogen and the metal atoms at a local atomic level is of utmost importance for the optimization of their properties.

Identifying the electronic character and the chemical environment of hydrogen in metal hydrides remains a key challenge in research focused on energy materials,

*panaccione@iom.cnr.it

†a.regoutz@ucl.ac.uk

Published by the American Physical Society under the terms of the [Creative Commons Attribution 4.0 International](https://creativecommons.org/licenses/by/4.0/) license. Further distribution of this work must maintain attribution to the author(s) and the published article's title, journal citation, and DOI.

catalysis, and gas-storage technology. Longstanding questions remain over (i) whether hydrides should be considered as predominantly ionic or covalent and (ii) the location of hydrogen-derived states in the d band of the metal or in the energy gap of the corresponding oxides [9]. Moreover, the strength and stability of the metal-hydrogen bond, as influenced by the possible formation and/or coexistence of other phases (e.g., oxides and hydroxides), defects, and by long-range diffusion of hydrogen atoms over the hydride thickness, is an essential parameter to be characterized and controlled.

Hydrogen presents a formidable challenge for many characterization techniques, with very few having sensitivity to its chemical states and bonding or being able to detect hydrogen-induced modifications on the electronic states directly [10,11]. One such technique is photoelectron spectroscopy (PES), which also has the added value of being nondestructive [12]. PES is frequently regarded as being “blind” to hydrogen, given that it has one electron and no available core line needed for chemical-state analysis. However, this is misleading, as the effect of hydrogen can be observed in the core levels of elements that are bonded with hydrogen. This has enabled PES-based studies to capture many relevant characteristics of metal hydrides to date [9,13–26]. Observations include (i) their high surface reactivity and formation of detrimental stable intrinsic oxides (influencing their catalytic properties) [16] and (ii) the changes in the electronic character of the extended valence states upon formation of the hydrides [influencing their (semi)metallic or semiconducting behavior] [13,18]. However, these results are predominantly obtained with highly surface-sensitive methods, including ultraviolet or soft x-ray electron emission excitation. As metal hydrides are extremely reactive, with their surfaces prone to oxidation under ambient conditions, it is challenging to disentangle the contribution from surface overlayers from those intrinsic to the hydride itself. A precise quantitative determination of both the thickness-dependent composition of surface oxides, hydroxides, and/or hydrides and the concentration and/or gradient of hydrogen-related features remains challenging, leaving significant uncertainties in the understanding of hydrides both experimentally and theoretically.

Synchrotron-based PES, particularly hard x-ray photoelectron spectroscopy (HAXPES), provides tunability of the photon energy, enabling access to a range of photon energies within the hard-x-ray regime. This allows for both the probing depth and the photoionization cross sections to be manipulated, with the latter enhancing the sensitivity to specific orbital states [27–34]. Regarding the application of HAXPES to metal dihydrides, the increase in probing depth with HAXPES over traditional soft x-ray PES enables the study of truly bulklike hydrides, as the contribution from the surface, which is expected to be metal oxide rich, is minimized. The probing-depth advantage

also removes constraints on the samples, as past studies using soft-x-ray PES have often needed samples to be cleaved or grown *in situ* to avoid surface oxidation. HAXPES is well suited for measuring realistic and technologically relevant samples with no surface preparation, as in the present case, where thin films of prototypical metal hydrides have been grown *ex situ* on specific substrates.

This work exploits the bulk sensitivity of HAXPES to probe the electronic structure of metal-hydrogen states of two technologically relevant metal dihydrides: titanium dihydride ($\text{TiH}_{2-\delta}$) and yttrium dihydride ($\text{YH}_{2-\delta}$). By exploiting photon-energy-dependent core-level analysis, pure-hydride states can be disentangled from oxide and hydroxide species and a nondestructive depth profile of the chemical states is obtained. Analysis of the valence-band (VB) spectra and comparison to theoretical models from density functional theory (DFT) allows the identification of metal-hydrogen states, as well as the specific contribution of metal d versus sp states near the Fermi energy (E_F). Moreover, this work discusses the empirical model proposed by Griessen and Driessen [35], which correlated the enthalpy of formation (ΔH_f) of metal dihydrides with a characteristic energy of the electronic structure of the host metal. Here, their model is extended and it is shown that the ΔH_f of metal dihydrides can be directly extracted from their HAXPES VB spectra.

II. METHODS

A. Synthesis

$\text{YH}_{2-\delta}$ and $\text{TiH}_{2-\delta}$ thin films with a thickness of approximately 200 nm were prepared by reactive magnetron sputtering of a 2-in. metal target (MaTeck Germany, 99.99% purity) in an Ar- H_2 atmosphere. Before deposition, the chamber was kept at a base pressure below 1×10^{-6} mbar. During deposition, two independent mass-flow controllers were used to define the composition of the gas mixture while the total deposition pressure was set to 3×10^{-3} mbar by means of a reducing valve mounted at the inlet of the pumping stage. An Ar: H_2 gas ratio of 7:1 and 7:2 was used for the deposition of the $\text{YH}_{2-\delta}$ and $\text{TiH}_{2-\delta}$ films, respectively. In both cases, plasma excitation was sustained with a total power of 200 W, supplied as direct current. All samples were grown on p -doped $< 100 >$ Si substrates without active heating and stored under an argon environment in a sealed container until the measurements were commenced.

B. Characterization methods

Energy-dependent HAXPES experiments were conducted at the HAXPES end station of Beamline P22 at PETRA III (DESY, Hamburg, Germany) [36]. All samples were prepared within an argon-filled glove box and

mounted on adhesive carbon tape. The samples were transferred into the HAXPES end station under an argon atmosphere to avoid exposure to air. Four photon energies were used—2.4106, 3.2691, 6.0054, and 7.2310 keV: these are referred to as 2.4, 3.3, 6.0, and 7.2 keV throughout the paper for simplicity. For all energies, a Si(111) double-crystal monochromator (DCM) was used and the following post-channel-cut monochromators were employed to achieve the final energy resolutions: Si(220) at 3.3 keV and Si(333) at 6.0 and 7.2 keV. No post-channel-cut monochromator was used at 2.4 keV. The achieved total energy resolutions as determined from taking the 16% to 84% width (the 16/84% method) of the Fermi edge of a polycrystalline gold-foil reference (for the Fermi edge spectra, see Sec. I of the Supplemental Material [37]) were 280 meV (2.4 keV), 243 meV (3.3 keV), 242 meV (6.0 keV), and 202 meV (7.2 keV). The error associated with these resolution values is ± 20 meV owing to the errors associated with using the 16/84% method. The measurements were conducted with an x-ray incidence angle of 15° and near-normal emission geometry and the core-level and VB spectra were collected at a pass energy of 30 eV and a step size of 50 meV. The end station is equipped with a SPECS Phoibos 225HV analyzer, providing a $\pm 30^\circ$ -wide acceptance angle, and a high dynamic range delay-line electron detector. The base pressure of the end station is 5×10^{-10} mbar. The core-level and VB spectra were aligned to the intrinsic E_F of the sample. The core-level spectra were normalized to their respective areas, while the VB spectra were normalized to the area of the metal-hydride states adjacent to E_F . The spectral areas were determined in both cases after removing a Shirley-type background. The error associated with the quoted binding energy (BE) values of the core lines is ± 0.2 eV, which accounts for both the total energy resolution of the measurements and the inherent error associated with peak-fit analysis. The error associated with quoted relative atomic percentages is ± 0.5 at.%, owing to the error associated with peak-fit analysis. HAXPES measurements on Ti and Y metal foils were conducted at Beamline I09 of the Diamond Light Source (Harwell, UK). Details of these measurements can be found in Sec. II of the Supplemental Material [37].

C. Theoretical methods

Density functional theory (DFT) [38,39] calculations were performed using the CASTEP software package [40]. The calculations employed the Perdew-Burke-Ernzerhof (PBE) exchange-correlation functional [41] and norm-conserving pseudopotentials with 12 (11) valence electrons for Ti (Y), using a kinetic energy cutoff of 1100 eV. The calculations employed Monkhorst-Pack [42] k -point grids of $3 \times 3 \times 3$ for TiH_2 , $3 \times 3 \times 4$ for TiO_2 , $2 \times 2 \times 1$ for Ti_2O_3 , $6 \times 6 \times 6$ for YH_2 , and $2 \times 2 \times 2$ for Y_2O_3 , while the projected densities of states (PDOS) for TiH_2 ,

YH_2 and TiO_2 were calculated on a finer $12 \times 12 \times 12$ k -point grid and the PDOS for Ti_2O_3 was calculated on a $6 \times 6 \times 2$ k -point grid. The k -point grid for Y_2O_3 was kept the same for the PDOS calculation. PDOS calculations were also performed using the hybrid PBE0 functional [43] for the Ti-containing structures. The equivalent calculations for YH_2 and Y_2O_3 were prohibitively expensive due to the larger unit-cell sizes. The cubic crystal structure was used for the calculations for both TiH_2 and YH_2 . An additional calculation was performed using the tetragonal crystal structure for TiH_2 and very minor differences are observed compared to the calculations with the cubic crystal structure (for a comparison between the PDOS spectra of TiH_2 using the cubic and tetragonal crystal structures, see Sec. III of the Supplemental Material [37]). Therefore, only the results from the calculations using the cubic structure will be discussed in this work. For all structures, both the atomic coordinates and cells were relaxed, imposing symmetry and using a maximum force tolerance of 0.02 eV/Å. The PDOS, atomic charges, and bond (overlap) populations were calculated using a Mulliken-based approach [44–46], while the atomic charges were also calculated using both Hirshfeld [47] and Bader [48,49] population-analysis approaches for comparison. We note that the spilling parameter for all systems was below 0.2%, indicating that the atomic orbital basis set used to perform the projection was reasonably complete. Nonetheless, there are inherent uncertainties in projecting delocalized orbitals onto an atomic basis set, which also tend to be more severe for metallic systems, resulting in negative contributions to the PDOS, which are visible in the sum of the cross-section-weighted PDOS and the difference plots shown in Fig. 2. Gaussian smearing of 0.24 and 0.20 eV was applied to the PDOS to match the experimental broadening when measuring at 3.3 keV and 7.2 keV, respectively. For a tabulation of the lattice parameters of the relaxed structures, see Sec. IV of the Supplemental Material [37].

Postprocessing was performed using OptaDOS [50]. The PDOS was further processed by applying Scofield photoionization cross-section weighting factors [51,52] to each projected state and then aligning the PDOS to the theoretically calculated E_F . This provides a better comparison to the experiment and the PDOS were summed to generate a simulated spectrum (for the unweighted PDOS spectra, see Sec. V of the Supplemental Material [37]). The GALORE software package [53] was used to interpolate the Scofield cross-section tabulated data [51,52] to determine the one-electron-corrected photoionization cross sections at the 3.3- and 7.2-keV photon excitation energies. The occupied Y $5s$ –Ti $4s$ and Y $4d$ –Y $3d$ one-electron-corrected photoionization cross sections were used to weight the s and d PDOS for Y-Ti. Given that the material system is metallic, it would be expected that p -conduction-band states (i.e., Y $5p$ –Ti $4p$) would be pulled

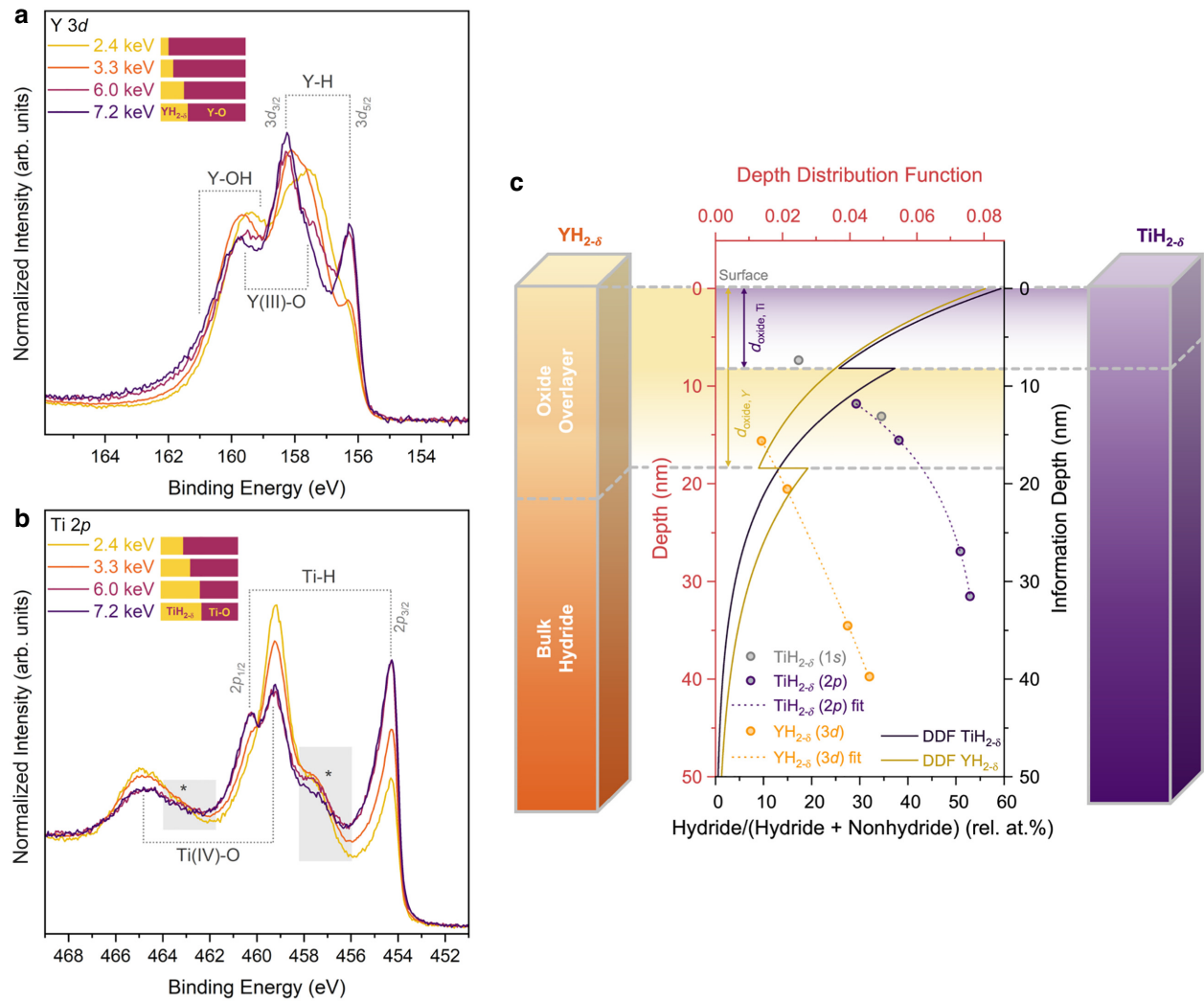


FIG. 1. The chemical states and the probing depth. (a),(b) Annotated core-level spectra of (a) $\text{YH}_{2-\delta}$ ($\text{Y } 3d$) and (b) $\text{TiH}_{2-\delta}$ ($\text{Ti } 2p$), respectively, as a function of the photon energy. The spectra are normalized to their respective areas (after removing a Shirley-type background) and plotted on a calibrated BE scale. An indication of the percentage split between the hydride (denoted as $\text{TiH}_{2-\delta}$ or $\text{YH}_{2-\delta}$) and nonhydride (denoted as Ti-O or Y-O for simplicity) contributions as determined from peak-fit analysis is included adjacent to the legends. The shaded regions in (b) containing an asterisk correspond to areas where additional lower-valence-state metal-oxide environments are present. (c) Estimation of the probing depth and the oxide-layer thickness. The evolution of the hydride intensity as a function of the information depth (black axes) of the respective core-level kinetic energies [integrating over 95% of the depth-distribution function (DDF)] for $\text{TiH}_{2-\delta}$ and $\text{YH}_{2-\delta}$. The solid lines show the DDF curves plotted as a function of the depth (red axes) and the data points represent the percentage contribution of the hydride components to the total spectral area determined from the $\text{Y } 3d$, $\text{Ti } 2p$, and $\text{Ti } 1s$ core-level spectra. Both depth axes—depth and information depth—are plotted on the same scale for ease of analysis. The horizontal shaded regions separated by dashed gray guidelines represent the estimated maximum oxide overlayer thickness, d_{oxide} . This value was determined using the DDF derived from the core-level spectra collected at $h\nu = 7.2$ keV. The oxide thicknesses were estimated to be 8.2 ± 2 and 18.4 ± 2 nm for $\text{TiH}_{2-\delta}$ and $\text{YH}_{2-\delta}$, respectively.

below the E_F and be responsible for the p -state contribution observed in the VB rather than the occupied $\text{Y } 4p$ – $\text{Ti } 3p$ shallow core-level states. As no photoionization cross sections are available for unoccupied states, the respective p one-electron-corrected cross sections were estimated

by dividing the s -orbital cross section by a factor of 2 [32,54]. The one-electron-corrected photoionization cross-section values used to weight the PDOS at both the 3.3- and 7.2-keV photon energies are tabulated in Section VI of the Supplemental Material [37].

III. RESULTS AND DISCUSSION

A. Analysis of chemical states and probing depth

The Y $3d$ and Ti $2p$ core levels collected at photon energies of 2.4, 3.3, 6.0, and 7.2 keV provide a nondestructive depth profile of the chemical states present in the metal-hydride films. The collected survey spectra, as well as additional core levels (O $1s$, Y $3p$, and C $1s$) and the deep Ti $1s$ core level, can be found in Secs. VII, VIII, and IX of the Supplemental Material [37], respectively. The survey spectra of both samples show all the expected elements, with dominant signals coming from Ti—Y. A significant

oxygen signal is also detected, owing to the unavoidable surface oxidation in realistic technologically relevant samples. Both $\text{YH}_{2-\delta}$ and $\text{TiH}_{2-\delta}$ films display a minor signal from carbon, which decreases in intensity with increasing photon energy, suggesting that it is constrained to the surface of the sample. Fluorine is also detected for $\text{YH}_{2-\delta}$ only and this stems from the synthesis route.

Figures 1(a) and 1(b) display the Y $3d$ and Ti $2p$ core-level spectra collected as a function of the photon energy for the $\text{YH}_{2-\delta}$ and $\text{TiH}_{2-\delta}$ films, respectively. The spectra are normalized to their respective spectral areas. In both cases, a clear evolution of the relative peak intensities is

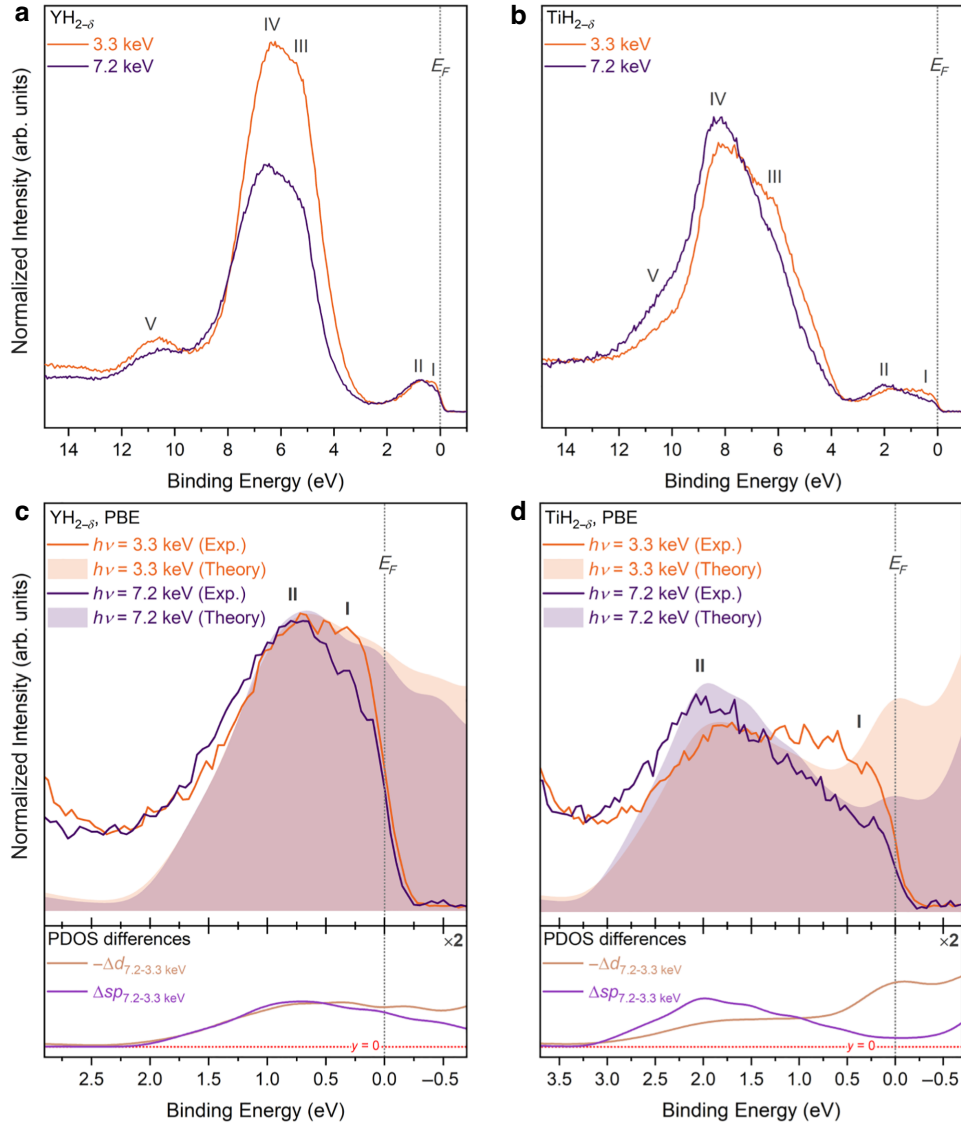


FIG. 2. The electronic structure of $\text{YH}_{2-\delta}$ and $\text{TiH}_{2-\delta}$. VB spectra collected at 3.3 and 7.2 keV are presented for (a) $\text{YH}_{2-\delta}$ and (b) $\text{TiH}_{2-\delta}$. These spectra are normalized to the total area of features I and II adjacent to the E_F . (c), (d) Magnified views of the density of states (DOS) adjacent to the E_F , along with a direct comparison with the total photoionization cross-section-weighted PDOS for (c) TiH_2 and (d) YH_2 , calculated with PBE (i.e., the sum of all PDOS). Underneath the main panels of (c) and (d) are the PDOS differences between the d and sp states when cross-section weighted at photon energies of 3.3 and 7.2 keV. Parts (a)–(d) are all plotted on the same y -axis scale but note the different x -axis scales. The PDOS differences at the bottom of panels (c) and (d) are plotted on a $\times 2$ magnified y -axis scale compared to the main-panel y -axis scale.

observed, with the lowest BE peak gaining more intensity as the photon energy increases, i.e., for larger probing depths [55]. This peak arises from the pure-metal-hydride states M—H, where M = Ti or Y. In good agreement with values previously reported in the literature for TiH₂ and YH₂ [9,19,56–58], the metal-hydride features appear at BEs of 156.4 eV for YH_{2-δ} (Y 3d_{5/2}) and 454.3 eV for TiH_{2-δ} (Ti 2p_{3/2}), both determined from peak-fit analysis of the spectra collected at 7.2 keV. These BE positions are higher than the expected BE positions of the pure-metal chemical states, which for Y and Ti metal are reported on average at 155.7 [9,19] and 453.9 eV [59,60], respectively. In a comparative study by Hayoz *et al.*, a +0.4 eV BE shift is observed for yttrium dihydride relative to hydrogen-free yttrium metal due to the electronic charge transfer from yttrium to hydrogen [19]. Additionally, they report that a shift of +1.5 eV from the pure metal represents a yttrium trihydride chemical state, while Riesterer reports a +0.5 eV shift for TiH_{1.9} relative to the pure Ti metal [18]. Given the existing literature and the fact that the present samples were fabricated under a constant Ar:H₂ gas ratio, it is clear that only metal dihydride chemical states are present, with both the pure-metal and higher-hydride species being absent from the spectra. A compilation of selected Ti 2p_{3/2} and Y 3d_{5/2} BE values reported in the literature for both Ti and Y in their metal, hydride, oxide, and hydroxide states can be found in Sec. X of the Supplemental Material [37]. Additionally, all spectra consistently show an asymmetric line shape for the dihydride states, as due to the metallic character and large population of states near the E_F of the hydrides, shake-up-like events occurring during electron core-level emission result in a higher BE tailing of the photoemission peak [61]. The asymmetric character was taken into account during the peak-fit analysis of the spectra as detailed in Sec. XI of the Supplemental Material [37].

Given that no *in situ* surface preparation was performed on the films, metal-oxide chemical states at higher BEs are expected as oxygen strongly interacts with hydrides, replacing hydrogen on the surface and forming an oxide overlayer. The hydrides studied here were deposited in the same manner as the samples detailed in Ref. [62] but without a palladium capping layer. In this reference, Rutherford back-scattering spectroscopy (RBS) measurements were performed and showed no traces of oxygen (i.e., below the detection limit of the technique) within the bulk or surface of the metal dihydride films. Therefore, the oxide found on the surface of these samples results from post-deposition oxidation rather than being due to any intrinsic oxygen incorporated during deposition. Due to the high reactivity of the hydrides, it can be assumed that the presence of residual oxygen present in either the load lock of the deposition chamber or the argon-filled transport setup is sufficient to lead to surface oxidation. To confirm this hypothesis, air-exposure tests were performed.

After the initial measurements, which will be referred to in the remaining discussion as “argon-transferred,” the samples were exposed to air for a short initial period (2 h) followed by long-term exposure (1 month). After both instances of air exposure, the samples were remeasured using the same photon energy (7.2 keV) and optics setup. A comparison of both the Ti 2p and Y 3d spectra collected without exposure to air and after both air-exposure time scales can be viewed in Sec. XII of the Supplemental Material [37]. The spectra appear almost identical across all measurements despite the significant air exposure. Assuming that the samples are homogeneous across the entire surface, the hydride-to-oxide peak intensities remain consistent over time, with only a slight decrease in the M—H signal intensity observed after extensive air exposure (less than 5 rel. at.% decrease in the hydride/(hydride + nonhydride) signal intensity between the argon-transferred and 1 month air-exposed spectra). The lack of significant change indicates that a stable passive oxide layer was already present in the samples after transporting them under argon before the initial HAXPES measurements, covering the sample surface and protecting the metal-hydride bulk.

The Y 3d spectra displayed in Fig. 1(a) show two chemical environments in addition to the metal-hydride state. First, there is an intense yttrium oxide feature (i.e., Y₂O₃-like), labeled as Y(III)-O, with the Y 3d_{5/2} peak at 157.5 eV (determined from the peak-fit analysis of the spectrum collected at 2.4 keV), agreeing with past reported values of the same chemical environment [63,64]. Second, there is a minor metal-hydroxide environment at even higher BEs, labeled as Y—OH. Such high-BE Y states are often attributed to metal hydroxide, other hydroxylated species, and metal carbonates [65,66]. As the C 1s core-level spectra show no detectable evidence of carbonate states and the O 1s spectra show a clear hydroxide feature on the higher-BE side of the main metal-oxide signal (for the C 1s and O 1s spectra, see Sec. VIII of the Supplemental Material [37]), it is clear that in the present case, the features in the Y core level arise from hydroxide species.

From peak-fit analysis of the Y 3d spectra, the metal-hydride contribution to the total spectral area was determined, with bar charts representing this ratio displayed adjacent to the legend in Fig. 1(a). The ratio was determined by comparing the raw spectral areas of the Y 3d_{5/2} peaks of each environment (i.e., without any escape-depth correction). Details regarding the methods used to peak fit the Y 3d core level can be found in Sec. XI of the Supplemental Material [37]. Due to the chemical shift between the hydride and all other chemical states, as well as the depth sensitivity of HAXPES, it is possible to disentangle the contributions from the bulk hydride and oxide overlayer, with the hydride contribution increasing while the oxide contribution reduces with increasing photon energy. Although a greater probing depth is provided

with increasing photon energy, oxygen-containing environments always dominate, with the hydride contribution increasing from 9.5 to 32.0 rel. at.% when going from 2.4 to 7.2 keV photon energy. This suggests that a thick oxide overlayer is present and this observation will be discussed further toward the end of this section.

The Ti $2p$ spectra displayed in Fig. 1(b) are similarly complex, owing to the mixture of both hydride and oxide environments. The main peak close to the center of the spectra is attributed to titanium oxide in the +4 oxidation state (i.e., TiO_2 -like) [60,67,68], labeled as Ti(IV)—O, with the doublet assigned to this environment appearing at BEs of 459.3 ($2p_{3/2}$) and 465.0 eV ($2p_{1/2}$), determined from the peak-fit analysis of the spectrum collected at 7.2 keV. Peak-fit analysis reveals the presence of additional lower-valence-state metal-oxide environments, which are labeled in Fig. 1(b) with an asterisk, appearing on the lower-BE side of the main Ti(IV)—O core lines [67,69]. As used for the Y $3d$ spectra, bar charts representing the hydride-to-nonhydride composition from peak fits of the Ti $2p_{3/2}$ lines are placed adjacent to the legend. Comparing the two systems, a significantly greater metal-hydride contribution to the total signal was detected for the $\text{TiH}_{2-\delta}$ sample. The Ti dihydride contribution at 2.4 keV (29.2 rel. at.%) almost matches the value obtained for Y dihydride at 7.2 keV. This rises to 52.9 rel. at.% when measured at a photon energy of 7.2 keV. Details regarding the methods used to peak fit the Ti $2p$ core level can be found in Sec. XI of the Supplemental Material [37]. The high-BE Ti $1s$ core level collected at 6.0 and 7.2 keV corroborates these findings (for the Ti $1s$ spectra and the peak fitting and analysis, see Secs. IX and XI of the Supplemental Material [37], respectively).

From the qualitative analysis of the core-level spectra collected as a function of the photon energy, the layer sequence of the hydride films and their overlayers becomes clear, as indicated in the bar charts in Figs. 1(a) and 1(b). Taking the depth information provided by HAXPES a step further, Fig. 1(c) offers a quantitative estimate of the oxide thickness as extracted from the Ti $2p$ and Y $3d$ core-level spectra using a depth-distribution function (DDF). The DDF estimates the probability of a photoelectron leaving the surface of a material having originated from a given depth measured normally from the surface. To calculate the DDF, the approach taken by Berens *et al.* was followed [70]. This approach is based on a bilayer, whereby the metal hydride is the bottom layer, which is covered by a homogeneous oxide overlayer. The required input parameters to the DDF are (a) the inelastic mean free path (IMFP) of the photoelectrons originating from their respective layers and travelling through their respective materials, (b) the number densities of both layers, and (c) an estimate of the percentage of the signal originating from each layer. Two assumptions have had to be made for calculating the DDF, namely (i) that the hydrides are stoichiometric TiH_2 and

YH_2 and (ii) that the metal-oxide overlayer is composed of the highest-valence oxidation state only (i.e., TiO_2 and Y_2O_3) and all nonhydride contributions to the spectral area are grouped together to represent the metal oxide. The relativistic IMFP was calculated using the TPP-2M predictive formula embedded in the QUASES-IMFP-TPP2M Ver. 3.0 software package [71]. The software already had TiO_2 and Y_2O_3 within its database but not the metal dihydrides and so the hydrides were entered into the software as new materials. A full description of the methodology, input values, approximations, and assumptions used for calculating the DDF can be found in Sec. XIII of the Supplemental Material [37]. The DDF was calculated at each photon energy, with the DDF for 7.2 keV displayed in Fig. 1(c) and used to estimate the oxide overlayer thickness. The value of 7.2 keV was selected on the basis that the hydride and non-hydride environments within the core-level spectra measured at this photon energy were better resolved than the spectra collected at lower photon energies, thereby reducing the error associated with the calculation. Figure 1(c) shows an increase in the metal-hydride contribution as the probing depth increases. The discontinuity in the DDF is due to the hydride and oxide having different bulk densities and atomic masses (i.e., number densities). At each photon energy, the information depth of the Y $3d$ and Ti $2p$ electrons was determined by integrating the area under the bilayer DDF curve and finding the depth that equated to 95% of the total area. This value is reported on the y axis of the graph. The x axis is the hydride/(hydride + nonhydride) composition.

From the 7.2-keV-derived DDF, the maximum oxide-layer thickness can be estimated as 8.2 ± 2 and 18.4 ± 2 nm for $\text{TiH}_{2-\delta}$ and $\text{YH}_{2-\delta}$, respectively, as schematically shown from the 3D blocks on the left and right sides that describe the sample structure. This thickness was determined by finding the information depth of the discontinuity of the DDFs, which signifies the interface of the oxide-hydride bilayer. The difference in oxide thickness is related to differences in the oxygen solubility and oxygen diffusivity of the two bulk hydrides, which are directly influenced by the metal [72,73]. Previous reports show that Ti has a low oxygen diffusivity and a high oxygen solubility, while the opposite is true for Y [73]. This translates to a greater diffusion length of oxygen in Y compared to Ti, leading to a significantly thicker oxide layer to form on $\text{YH}_{2-\delta}$. This will considerably influence the behavior of these two metal hydrides in applications and native-oxide overlayer thicknesses should be considered when comparing the performance of different metal-hydride samples.

B. Electronic structure and bond nature

Analysis of the core states and observation of the depth distribution of hydride versus nonhydride chemical states

promises the possibility of also observing metal-hydride states in the VB and, in particular, close to the E_F . It is important to emphasize that the analysis of VB spectra in solids is complex. While core-level BEs are well separated for different chemical species and oxidation states, valence states are superimposed and weighted with both depth sensitivity and photoionization cross sections [74]. Figures 2(a) and 2(b) display the VB spectra of the $YH_{2-\delta}$ and $TiH_{2-\delta}$ films, respectively, collected at photon energies of 3.3 and 7.2 keV (VB spectra and shallow core-level spectra collected at all four-photon energies are included in Secs. XIV and XV of the Supplemental Material [37], respectively). The spectra are normalized to the spectral area of features I and II. They show several clearly identifiable features, including (I) 0.4, (II) 0.8, (III) 5.5, (IV) 6.8, and (V) 10.5 eV for $YH_{2-\delta}$ and (I) 0.8, (II) 2.0, (III) 6.4, (IV) 8.3, and (V) 10.2 eV for $TiH_{2-\delta}$. By combining the photon-energy-dependent experimental spectra with cross-section-weighted projected density of states (PDOS) calculations (for the 3.3- and 7.2-keV-weighted PDOS spectra, see Secs. XVI and XVII of the Supplemental Material [37], respectively), it is possible to disentangle the individual orbital contributions to these features.

Starting with $YH_{2-\delta}$ shown in Fig. 2(a), the spectra are in good agreement with past experimental VB spectra collected by Fujimori and Schlappbach for $YH_{2.1}$ ($h\nu = 1253.6$ eV (Mg $K\alpha$) [9] and by Weaver *et al.* for YH_2 ($h\nu = 18 - 35$ eV) [13]. Notably, we observe a density of states (DOS) adjacent to E_F (in the BE region up to 2.0 eV) similar to the aforementioned studies. Fujimori and Schlappbach identified two main features at 5.5 eV and within 2.0 eV of the E_F , attributing them to a hydrogen-induced band and the Y $4d^1$ conduction band, respectively [9]. In the present case, the core-level spectra show that metal-oxide states will also contribute to the VB spectra. However, features I and II can unequivocally be assigned to yttrium hydride states, as (i) yttrium oxide has a band gap of approximately 5.6 eV and therefore does not have any states in this BE region [25,75–78] and (ii) the core-level spectra exclude the presence of yttrium metal. Weaver *et al.* highlight that if such features are present in the VB spectrum, then this is further evidence of a metal dihydride specifically rather than a mono- or trihydride system [14,79].

The higher-BE features III and IV in the $YH_{2-\delta}$ spectra have contributions from both the metal hydride [9,13] and metal-oxide states [17]. Given that features I and II are metal hydride related and that the VB spectra are normalized to these features, the clear decrease of both features III and IV with higher photon energies agrees with the expected decrease of the surface metal-oxide contribution upon increasing information depth. Feature V is not described by the PDOS for either the metal hydride or the corresponding oxide but is commensurate with surface hydroxyl groups. This also agreed with the observation of

a minor Y—OH environment in the Y $3d$ core level [see Fig. 1(a)]. Furthermore, alternative explanations in the literature include surface states [80], yttrium-hydrogen [81], or yttrium-carbon [82] contributions. The cross-section-weighted PDOS of the metal oxides can also be found in Secs. XVI and XVII of the Supplemental Material [37].

In parallel to the analysis of $YH_{2-\delta}$, $TiH_{2-\delta}$ has a similar VB structure, as shown in Fig. 2(b). Features I and II can again be attributed solely to titanium hydride-derived bands, owing to the approximately 3.0 eV band gap of TiO_2 [83]. The presence of such features as highlighted by Weaver *et al.* also confirms that a titanium dihydride system is present. It is noted that the BE-region width encompassing features I and II is approximately 1 eV larger for $TiH_{2-\delta}$ compared to $YH_{2-\delta}$. This widening is thought to stem from the difference in the valence state of the two hydrides, with $TiH_{2-\delta}$ being tetravalent and $YH_{2-\delta}$ being trivalent [79]. Weaver *et al.* observed the same trend when comparing the width of states that fall near E_F for $YH_{1.98}$ and $ThH_{1.91}$, with the latter being tetravalent, similarly to $TiH_{2-\delta}$ in our case [79]. It is worth noting that in-gap electronic states have been reported in titanium oxide at BEs close to those of structures I and II [84–86]. However, such states have a single-peak shape with d orbital symmetry only and are limited to the very top surface. Since the spectra presented here probe a large depth in the material and the structured conduction-band spectra show a different orbital character [Figs. 2(c) and 2(d)], the contribution of in-gap states in the energy region of structures I and II, if present, is negligible. Features III, IV, and V in the $TiH_{2-\delta}$ spectra are analogous to the same numbered features in the $YH_{2-\delta}$ spectra.

The unweighted theoretical spectra calculated with DFT are displayed in Sec. V of the Supplemental Material [37]. The PDOS for TiH_2 has the center of the H $1s$ state at an energy of 5.6 eV below E_F , while it is at 4.3 eV for YH_2 . This is commensurate with the energy-band diagram and DOS of TiH_2 reported by Gupta [14,87] and Smithson *et al.*, [88], respectively, where a hydrogen-induced band is centered around 6 eV from E_F , and with the DOS calculated for YH_2 by Peterman *et al.*, wherein they report the equivalent band at approximately 4 eV below E_F [89]. This further confirms that a hydrogen-induced state will contribute to feature III in the experimental VB spectra for both dihydrides. Furthermore, the PDOS show that compared to $YH_{2-\delta}$, the VB states in $TiH_{2-\delta}$ span a wider BE range. This leads to the bottom of the VB overlapping with feature V in the experimental VB spectra, which is assumed to arise from surface states and adsorbed species. Other notable theoretical works on these two metal dihydride systems can be found in Refs. [26,90–92] and are in good agreement with the results obtained here.

Returning to a more detailed discussion of features I and II, Figs. 2(c) and 2(d) display magnified views of the experimental and theoretical VB spectra along

with the corresponding cross-section-weighted PDOS calculations in the bottom panel for $\text{YH}_{2-\delta}$ and $\text{TiH}_{2-\delta}$, respectively. One noteworthy aspect of the comparison between theory and experiment throughout this work is that both are aligned to their respective intrinsic E_F values. No additional alignment was needed, as is often the case due to challenges in obtaining absolute energy scales from theory or fully trustworthy energy alignments in experiments. The exceptional quality of the agreement between experiment and theory for the hydrides is further compounded by changes in experimental intensity near the E_F , with the photon energy being clearly reflected in the photoionization cross-section-corrected PDOS.

The drop in intensity at higher photon energy is not constant across features I and II but a stronger drop at the top of the VB (feature I) is noticeable. This is due to differences in the photoionization cross sections, where d states decrease at a higher rate relative to both s and p states at higher photon energies. From the complete cross-section-weighted PDOS at 3.3 and 7.2 keV (see Secs. XVI and XVII of the Supplemental Material [37], respectively), Y $5s$ (Ti $4s$) states contribute to feature II. In contrast, feature I has contributions from both Y $4d$ (Ti $3d$) and Y $5p$ (Ti $4p$) states. The net decrease of feature I at higher photon energy with respect to feature II suggests a larger d -state contribution compared to p states, pointing to a sd -hybridization scheme, with only marginal participation of the p orbitals. This reflects a more complex bonding situation in these hydrides than previously thought, in that not only does the metal d -derived band contribute to the energy region within 3.0 eV from the E_F , as suggested by

Weaver *et al.* for both group III B [13] and group IV B [14] transition-metal dihydrides, but that extended s and p states are also important [9].

The excellent agreement between experiment and theory in the electronic structure analysis allows further use of DFT to examine the bonding nature of the metal hydrides. The electron densities extracted from the DFT calculations of the two hydrides, depicted in Fig. 3, show a clearly localized density around the atoms, indicating an ionic or metallic bonding nature. This can be examined in more detail by considering the atomic charges and overlap (bond) populations (for these values, see Sec. XVIII of the Supplemental Material [37]). A similar approach was taken by Yang *et al.* to assess the effects of alloying on the chemical bonding of TiH_2 [93]. The absolute values for both quantities are not themselves meaningful, particularly in the case of metallic systems, as illustrated by variations between absolute atomic charges calculated using different population-analysis approaches (Mulliken, Hirshfeld, and Bader). It is nonetheless possible to extract useful information about the trends [45,46].

The overlap bond population is lower for the M—H bond than for the M—O bond in all cases (Ti, Y, and PBE/PBE0 where applicable), with some variation between the different M—O populations. This signifies that both hydrides are more ionic than their corresponding oxides. This is further evidenced by the atomic charges, where for all three of the considered population-analysis approaches, the effective valence is smaller for the hydrides than the corresponding oxide. This implies a more ionic bonding nature for the hydrides compared to the more covalent nature of the oxides.

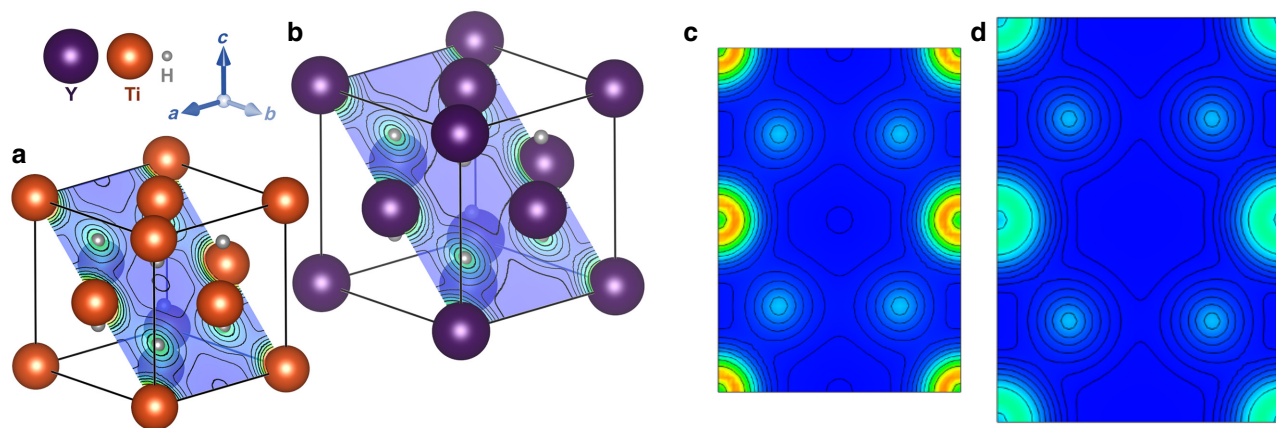


FIG. 3. The bond nature of metal hydrides. Using the relaxed TiH_2 and YH_2 structures (calculated with PBE), electron-density maps were obtained, with (a) and (b) showing the 3D density maps for TiH_2 and YH_2 , respectively. Two-dimensional (2D) electron-density maps for TiH_2 and YH_2 are displayed in (c) and (d), respectively. The 2D electron-density maps are plotted along the (011) body-diagonal lattice plane (1 d from the origin) and on the same intensity scale to allow for a direct comparison. Note that the 3D maps are for reference only, to show where the 2D maps have been extracted from (the color scale does not match the 2D maps). Contour lines have been added to the 2D electron-density maps. These contour lines have been plotted using the function $F(N) = A \times B^{N/\text{step}}$, where $A = 1$, $B = 10$, $N_{\min} = -1$, $N_{\max} = 3$, and $\text{step} = 5$. The maps are temperature scaled, with the blue regions indicating a low electron density and the red regions indicating a high electron density.

While the overall bonding nature of both hydrides is clear, a direct comparison between the two is complicated. Using the 2D density maps displayed in Figs. 3(c) and 3(d), a visual inspection of the densities suggests a more diffuse density on the metal atoms in YH₂ compared to TiH₂; however, the differences are subtle. The overlap populations support this picture, being slightly smaller in TiH₂, suggesting that TiH₂ is more ionic than YH₂. However, the atomic charges indicate the opposite, with YH₂ having a smaller effective valence than TiH₂. This difference is small for the Hirshfeld and Mulliken approaches but more significant for Bader. In other words, while the results clearly indicate that the hydrides exhibit an ionic bonding nature compared to the more covalent nature shown in the oxides, they are inconclusive about which of the two hydrides is more ionic. This is perhaps not surprising, given the small differences in electronegativity of the two metals (1.5 for Ti and 1.2 for Y). Using this as an indication to determine the ionic versus covalent bonding nature of the two systems [94,95], the bonds in both hydrides can be classified as metallic or partial ionic and partial metallic bonds [96]. In contrast, the larger overlap population in YH₂ compared to TiH₂ suggests a stronger bond in the former, as indeed reflected by the obtained values of enthalpy of formation of the two compounds, which are larger in YH₂ than in TiH₂ [97,98].

C. Enthalpy of formation

The enthalpy of formation, ΔH_f , is a highly relevant value for determining the hydrogen-storage capability in a metal hydride [99]. The absorption or desorption plateau pressure p_{H_2} for two-phase metal-hydrogen systems can be related to ΔH_f via the van 't Hoff equation [100]:

$$\ln p_{H_2} = \frac{\Delta H_f}{RT} - \frac{\Delta S}{R}, \quad (1)$$

where R is the universal gas constant ($8.314 \text{ J mol}^{-1} \text{ K}^{-1}$), T is temperature, and ΔS is the change in entropy for H₂ absorption. Therefore, a larger negative enthalpy of formation indicates that a hydride phase can be formed at lower hydrogen partial pressures as desired. Griessen and Driessen have proposed an empirical linear relationship between the enthalpy of formation of metal hydrides and the characteristic energy, ΔE , in the electronic band structure of the host metal [35]:

$$\Delta H_f = \frac{n_s}{2}(\alpha \Delta E + \beta), \quad (2)$$

where $\Delta E = E_s - E_F$, $E_F = 0 \text{ eV}$, E_s is the center of the lowest conduction band of the host metal and is equivalent to the energy at which the integrated density of states ($\int \text{DOS}$) of the host metal is equal to $0.5n_s$, n_s is the number of electrons per atom in the lowest s -like conduction band of the host metal, $\alpha = 29.62 \text{ kJ/eV mol H}$, and

$\beta = -135 \text{ kJ/mol H}$ [35]. For alkali metals, n_s is equal to one, but for all other metals (including Ti and Y), n_s is equal to two. Therefore, for Y and Ti, E_s is the energy at which the $\int \text{DOS} = 1$. The α and β terms were derived by Griessen and Driessen by correlating the ΔE values determined by integrating the total DOS of the host metal to the measured values of ΔH_f values found in the literature (see Ref. [35, Fig. 4]). The authors claimed that the use of ΔE derived in this way was effective in reproducing the measured ΔH_f values. However, it is noted that there is a large degree of scatter in Ref. [35, Fig. 4] the paper used to determine the α and β terms, as well as multiple different ΔH_f entries for the same metal, raising some concerns about the robustness of the model and the accuracy of the α and β terms.

Relevant to this work, Griessen and Driessen used their model approach to derive the enthalpy of formation of TiH₂ and YH₂. Using the calculated electronic band structures of Ti and Y metal available at the time of the publication of Ref. [35], they determined ΔE for Ti and Y metal to be 2.41 and 1.47 eV, respectively. These values are displayed on the left-hand side of Fig. 4(a) and inputting them into Eq. (2) gives ΔH_f values of -63.6 and -91.5 kJ/mol H for TiH₂ and YH₂, respectively (shown by viewing the right y -axis scale on Fig. 4). These ΔH_f values deviate significantly from experimental values reported in the literature, which are displayed in Fig. 4 as light dashed lines ($\Delta H_{f, YH_2} = -112.25 \text{ kJ/mol H}$ (between 873 and 1073 K) [98], $\Delta H_{f, YH_2} = -112.5 \text{ kJ/mol H}$ [97], $\Delta H_{f, TiH_2} = -63.0 \text{ kJ/mol H}$ [97], $\Delta H_{f, TiH_2} = -68.47 \text{ kJ/mol H}$ (at 737 K) [101,102]). To compensate for this, the authors devised ‘‘optimized’’ ΔE values (see Ref. [35, Table II]) to reproduce a better match with experimental values of ΔH_f . These optimized values are displayed on the right-hand side of Fig. 4(a). Using the optimized values, a better match to the ΔH_f literature values was then obtained for YH₂ but not for TiH₂ and this is because of an error associated with the ΔH_f value of TiH₂ used by the authors, which does not match modern values.

The enthalpy of formation can be obtained directly from theoretical calculations and DFT has been employed to calculate this property for metal dihydrides previously [88,103–106]. Here, the approach detailed in Ref. [103] was used to obtain values for titanium and yttrium dihydride. This approach required additional calculations of H₂ and bulk Ti and Y metal, with further details of the calculations and methods described in Sec. XIX of the Supplemental Material [37]. The resulting enthalpies of formation for titanium and yttrium dihydride are -71.4 and -105.6 kJ/mol H , respectively. Reasonable agreement with the literature is found, with the titanium dihydride DFT-determined enthalpy being slightly overpredicted compared to the literature value and the opposite being true for the yttrium dihydride case.

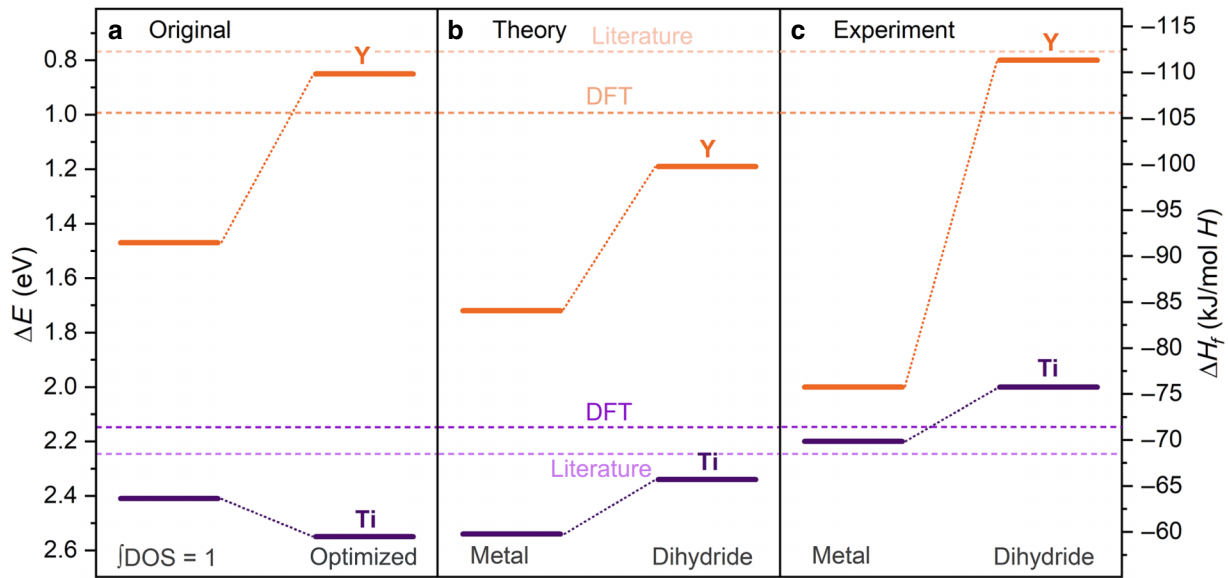


FIG. 4. The enthalpy of formation. A comparison between the ΔE values obtained by various methods (left y axis) and the resultant ΔH_f values calculated by inputting said ΔE values into Eq. (2) (right y axis). (a) On the left-hand side, the ΔE values extracted from Ref. [35, Fig. 4] are displayed. These values, termed “Original,” were determined by the authors of Ref. [35] by calculating the energy where the integrated total DOS of the host metal was equal to one. On the right-hand side of (a), the optimized ΔE values for Ti and Y taken from Ref. [35, Table II] are displayed. (b) ΔE values extracted from the PDOS of the metals and dihydrides calculated in this work and termed “Theory.” Abiding by the definitions of ΔE for the dihydrides, the position of the s band closest to E_F was used. For the metal, the main intensity s -state peak position was used to determine ΔE . (c) ΔE values determined using the position of feature II in the VB spectra collected with HAXPES and termed “Experiment.” For (b) and (c), the left-hand side displays the metal value and right-hand side the dihydride value. Horizontal dashed reference lines are plotted to indicate the enthalpy of formation determined using DFT (darker line) and reported in the literature (“Literature”) using experimental methods (lighter line).

While DFT calculations are incomparably more accessible today than at the time when Griessen and Driessen published their model, this direct calculation cannot link specific orbital character with the resulting values. Therefore, the theoretical PDOS and experimental HAXPES VB spectra of the host metals and metal dihydrides were obtained to extract ΔH_f values independently. This provides the opportunity to expand on the model by Griessen and Driessen and to explore if the enthalpy of formation of metal dihydrides can be derived using data other than the integrated total DOS of the host metal. It is recalled and directly quoted from Ref. [35] that E_s has “primarily s character with respect to the interstitial sites occupied by hydrogen atoms,” and “ n_s represents the number of electrons per atom in the lowest s -like conduction band of the host metal” [35]. Based on these quotes, the first approach was to use the position of the main s -state intensity in our calculated PDOS of the two host metals as the value of ΔE (for the unweighted PDOS of Ti and Y metal, see Sec. XX of the Supplemental Material [37]). Given that theory and experiment are referenced to an intrinsic E_F , E_s and ΔE will be used interchangeably in this work. The values of ΔE from the metal PDOS spectra are displayed on the left-hand side of Fig. 4(b). This expands

the application of Griessen and Driessen’s model, as they only had total DOS rather than individual PDOS available. However, comparing the resultant ΔH_f values to the values from the literature, it is clear that in both cases, the use of the main s -state intensity position significantly underestimates the values. This indicates that the model in its original form cannot be applied in this manner and, instead, requires optimization of the α and β terms. However, to generate optimized values of α and β , similar to the work in Ref. [35], a larger data set is required than the two metal systems studied in this work.

Upon hydriding, the host metal s band is known to be lowered due to the presence of hydrogen. For the case of a dihydride, this lowering is largely compensated by the increase in Coloumb energy due to the increased charge density around the protons [35]. However, alongside the lowering of the main metal s band some 4–8 eV below E_F , conduction-band states are also pulled below E_F [14]. Both phenomena are apparent when comparing the PDOS spectra of the host metal and the equivalent metal dihydride, which are included in Sec. XX of the Supplemental Material [37]. The position of the lowest-lying s band cannot be taken as the value of E_s , as it would give too large a ΔE value, resulting in a positive ΔH_f . Instead, if

the position of the conduction-band metal s state pulled below E_F is taken from the metal dihydride PDOS as ΔE , Fig. 4(b) shows that the ΔE value decreases with respect to the ΔE value from the s position in the metal PDOS. Consequently, when using these values in Eq. (2), the estimated ΔH_f values for TiH_2 and YH_2 are -65.7 and -99.8 kJ/mol H, which improve on the values determined using the metal s position from the metal PDOS. However, they do not provide a satisfactory agreement with the literature values.

Therefore, the HAXPES VB of the metal and metal dihydrides was used and applied to the model. While the metal-dihydride VB spectra are displayed in Fig. 2, the Ti and Y metal VB spectra are shown in Sec. II of the Supplemental Material [37]. For Ti and Y metal, the s -state intensity will be enhanced with HAXPES and by comparing the VB spectra collected with HAXPES to those in the literature collected with soft XPS or to PDOS calculations [9,25,107–110], feature II in both can be assumed to be s dominated and therefore can be taken as the value for E_s . Taking these positions [as displayed in Fig. 4(c)] gives ΔE values of 2.2 and 2.0 eV for Ti and Y, respectively, which again causes the ΔH_f value for YH_2 to be significantly underestimated compared to the literature value. At the same time, a good agreement is found for the TiH_2 estimation. This indicates that feature II in the Y metal VB spectrum is incorrect and cannot be used as E_s . The primary source of error here is that Y metal is incredibly difficult to keep clean due to its strong potential to react with oxygen and the VB spectrum is likely convoluted with oxygen-related states, leading to errors when selecting a feature for E_s .

Returning to the metal dihydride VB HAXPES spectra in Fig. 2, the PDOS identified that feature II exhibited the strongest s character. We find that using the position of feature II in the experimental VB as the value of E_s ($\text{YH}_{2-\delta} = 0.8$ and $\text{TiH}_{2-\delta} = 2.0$ eV) in Eq. (2), one obtains $\Delta H_{f,\text{YH}_{2-\delta}} = -111.3$ kJ/mol H and $\Delta H_{f,\text{TiH}_{2-\delta}} = -75.8$ kJ/mol H. These values, displayed in Fig. 4(c), compared to all other approaches discussed above, provide the best agreement with the experimental values reported in the literature. Section XXI of the Supplemental Material [37] tabulates the ΔH_f values calculated using Eq. (2) and the various values of ΔE .

Although the model by Griessen and Driessen was explicitly defined in their original paper [35] as being based on the electronic structure of the host metals, the agreement found here provides convincing evidence that from the experimental VB of a metal dihydride, one can infer the enthalpy of formation, as there is a clear link between the position of the s -state-dominated feature II and this critical property. To confirm this finding further, a library of metal dihydrides should be studied using HAXPES in the future, which will also allow the determination of new values of α and β .

IV. CONCLUSIONS

The combination of HAXPES-core and valence-photoelectron spectroscopy with theoretical spectra from DFT provides a powerful analytical approach to increase our understanding of metal hydrides. Photon-energy-dependent HAXPES delivers a nondestructive depth profile of $\text{YH}_{2-\delta}$ and $\text{TiH}_{2-\delta}$ thin films. From core-level analysis, it is shown that these samples can be modeled as a bilayer system consisting of a passive metal-oxide overlayer protecting the underlying metal hydride. By tuning the photon energy across the hard x-ray regime from 2.4 to 7.2 keV, the metal-hydride-related states can be probed and enhanced while minimizing any metal-oxide surface contributions. By extracting quantitative information from the Ti $2p$ and Y $3d$ core-level spectra and utilizing the depth-distribution model, quantitative estimates of the titanium and yttrium oxide layer thicknesses of 8.2 ± 2 and 18.4 ± 2 nm, respectively, were determined. Analysis of the valence spectra highlights the presence of metal-hydride-related states near the E_F . By comparing the experimental spectra and theoretical cross-section-weighted PDOS, the nature of hydride states close to E_F could be clearly identified as a combination of d and sp contributions. Exploiting photoionization cross-section effects with increasing photon energy, the importance of metal sp states near E_F alongside d states was identified. Finally, the bond character of the two metal-hydride systems was assessed, with the results suggesting that both are more ionic than their oxide counterparts. Additionally, the enthalpies of formation of -111.3 kJ/mol H for $\text{YH}_{2-\delta}$ and -75.8 kJ/mol H for $\text{TiH}_{2-\delta}$ were directly obtained from valence spectra using the model proposed by Griessen and Driessen, in good agreement with values determined using thermodynamical experimental methods. This remarkable result directly links the electronic structure and macroscopic properties fundamental for characterizing metal-hydrogen systems for energy-storage applications.

ACKNOWLEDGMENTS

C.K. acknowledges support from the Department of Chemistry, UCL. L.E.R. acknowledges support from an Engineering and Physical Sciences Research Council (EPSRC) Early Career Research Fellowship (EP/P033 253/1). A.R. acknowledges support from the Analytical Chemistry Trust Fund for her Community for Analytical Measurement Science (CAMS)—UK Fellowship. Parts of this research were carried out at Beamline P22 at DESY, a member of the Helmholtz Association (HGF). The research leading to this result has been supported by the European Union Horizon 2020 Framework Programme for Research and Innovation, through the project Convenient Access to Light Sources Open to Innovation (CALIPSO)plus, under Grant Agreement No. 730872.

Funding for the HAXPES instrument at Beamline P22 by the Federal Ministry of Education and Research (BMBF) under Contracts No. 05KS7UM1 and No. 05K10UMA with Universität Mainz, and Contracts No. 05KS7WW3, No. 05K10WW1, and No. 05K13WW1 with Universität Würzburg, is gratefully acknowledged. We would also like to acknowledge Dr. Volodymyr Baran for his assistance in preparing the samples in the glove box at DESY. We acknowledge Diamond Light Source for time on Beamline I09 under Proposal NT29451-3.

All authors contributed to the concept and design of the experiments. C.K., G.P., C.S., A.G., T.-L.L., P.K.T., and A.R. performed the synchrotron-radiation experiments, C.K., A.R., P.B., Y.Z., and F.O. analyzed the data, and G.C. and B.D. provided samples, growth, and characterization. L.R. performed the theoretical calculations. C.K., J.O., F.O., G.P., and A.R. drafted the paper, with input from all authors.

- [1] L. Schlapbach and A. Züttel, Hydrogen-storage materials for mobile applications, *Nature* **414**, 353 (2001).
- [2] J. M. Joubert, M. Latroche, and A. Percheron-Guégan, Metallic hydrides II: Materials for electrochemical storage, *MRS Bulletin* **27**, 694 (2002).
- [3] J. Bellosta von Colbe *et al.*, Application of hydrides in hydrogen storage and compression: Achievements, outlook and perspectives, *Int. J. Hydrogen Energy* **44**, 7780 (2019).
- [4] S. Yun and S. Ted Oyama, Correlations in palladium membranes for hydrogen separation: A review, *J. Memb. Sci.* **375**, 28 (2011).
- [5] J. Huijberts, J. Rector, R. Wijngaarden, S. Jetten, D. de Groot, B. Dam, N. Koeman, R. Griessen, B. Hjörvarsson, S. Olafsson, and Y. Cho, Synthesis of yttriumtrihydride films for ex-situ measurements, *J. Alloys Compd.* **239**, 158 (1996).
- [6] L. J. Bannenberg, C. Boelsma, K. Asano, H. Schreuders, and B. Dam, Metal hydride based optical hydrogen sensors, *J. Phys. Soc. Jpn.* **89**, 051003 (2020).
- [7] C. Langhammer, I. Zorić, B. Kasemo, and B. M. Clemens, Hydrogen storage in Pd nanodisks characterized with a novel nanoplasmonic sensing scheme, *Nano Lett.* **7**, 3122 (2007).
- [8] K. J. Palm, J. B. Murray, T. C. Narayan, and J. N. Munday, Dynamic optical properties of metal hydrides, *ACS Photonics* **5**, 4677 (2018).
- [9] A. Fujimori and L. Schlapbach, Electronic structure of yttrium hydride studied by x-ray photoemission spectroscopy, *J. Phys. C: Solid State Phys.* **17**, 341 (1984).
- [10] M. Malinowski, Some future directions for metal hydride surface studies: Electrons as probes of hydrogen, *J. Less Common Metals* **89**, 1 (1983).
- [11] Y.-S. Liu, S. Jeong, J. L. White, X. Feng, E. Seon Cho, V. Stavila, M. D. Allendorf, J. J. Urban, and J. Guo, In-situ/operando x-ray characterization of metal hydrides, *ChemPhysChem* **20**, 1261 (2019).
- [12] P. D. C. King, S. Picozzi, R. G. Egdell, and G. Panaccione, Angle, spin, and depth resolved photoelectron spectroscopy on quantum materials, *Chem. Rev.* **121**, 2816 (2021).
- [13] J. H. Weaver, D. T. Peterson, and R. L. Benbow, Electronic structure of metal hydrides. III. Photoelectron spectroscopy studies of ScH₂, YH₂, and LuH₂, *Phys. Rev. B* **20**, 5301 (1979).
- [14] J. H. Weaver, D. J. Peterman, D. T. Peterson, and A. Franciosi, Electronic structure of metal hydrides. IV. TiH_x, ZrH_x, HfH_x, and the fcc-fct lattice distortion, *Phys. Rev. B* **23**, 1692 (1981).
- [15] L. Schlapbach and J. Osterwalder, XPS studies of the valence band and of the 4f and 3d levels of Ce hydrides, *Solid State Commun.* **42**, 271 (1982).
- [16] R. A. Butera, J. H. Weaver, D. J. Peterman, A. Franciosi, and D. T. Peterson, Hydrogen diffusion and hydride formation at the metal-hydride interface, *J. Chem. Phys.* **79**, 2395 (1983).
- [17] J. Osterwalder, On the electronic structure of the light rare earth hydrides, *Z. Phys. B Condens. Matter* **61**, 113 (1985).
- [18] T. Riesterer, Electronic structure and bonding in metal hydrides, studied with photoelectron spectroscopy, *Z. Phys. B Condens. Matter* **66**, 441 (1987).
- [19] J. Hayoz, T. Pillo, M. Bovet, A. Züttel, S. Guthrie, G. Pastore, L. Schlapbach, and P. Aebi, Preparation and characterization of clean, single-crystalline YH_x films (0 ≤ x ≤ 2.9) on W(110), *J. Vac. Sci. Technol., A: Vacuum, Surfaces, and Films* **18**, 2417 (2000).
- [20] J. Hayoz, J. Schoenes, L. Schlapbach, and P. Aebi, Switchable yttrium-hydride mirrors grown on CaF₂(111): A x-ray photoelectron spectroscopy and diffraction study, *J. Appl. Phys.* **90**, 3925 (2001).
- [21] J. Hayoz, C. Koitzsch, D. Popović, M. Bovet, D. Naumović, and P. Aebi, Angle-scanned photoemission on YbH_x: Relevance for switchable mirrors, *Surf. Rev. Lett.* **9**, 235 (2002).
- [22] J. Hayoz, C. Koitzsch, M. Bovet, D. Naumović, L. Schlapbach, and P. Aebi, Electronic Structure of the YH₃ Phase from Angle-Resolved Photoemission Spectroscopy, *Phys. Rev. Lett.* **90**, 4 (2003).
- [23] M. Uno, K. Yamada, T. Maruyama, H. Muta, and S. Yamanaka, Thermophysical properties of zirconium hydride and deuteride, *J. Alloys Compd.* **366**, 101 (2004).
- [24] S. Kato, A. Borgschulte, D. Ferri, M. Bielmann, J.-C. Crivello, D. Wiedenmann, M. Parlinska-Wojtan, P. Rossbach, Y. Lu, A. Remhof, and A. Züttel, CO₂ hydrogenation on a metal hydride surface, *Phys. Chem. Chem. Phys.* **14**, 5518 (2012).
- [25] T. Mongstad, A. Thøgersen, A. Subrahmanyam, and S. Karazhanov, The electronic state of thin films of yttrium, yttrium hydrides and yttrium oxide, *Sol. Energy Mater. Sol. Cells* **128**, 270 (2014).
- [26] E. Billeter, Z. Łodziana, and A. Borgschulte, Surface properties of the hydrogen-titanium system, *J. Phys. Chem. C* **125**, 25339 (2021).
- [27] G. Panaccione, G. Cautero, M. Cautero, A. Fondacaro, M. Grioni, P. Lacovig, G. Monaco, F. Offi, G. Paolicelli, M. Sacchi, N. Stojic, G. Stefani, R. Tommasini, and P. Torelli,

- High-energy photoemission in silver: Resolving d and sp contributions in valence band spectra, *J. Phys.: Condens. Matter* **17**, 2671 (2005).
- [28] M. Sacchi, F. Offi, P. Torelli, A. Fondacaro, C. Spezzani, M. Cautero, G. Cautero, S. Huotari, M. Gioni, R. Delaunay, M. Fabrizioli, G. Vankó, G. Monaco, G. Paolicelli, G. Stefani, and G. Panaccione, Quantifying the effective attenuation length in high-energy photoemission experiments, *Phys. Rev. B* **71**, 1 (2005).
- [29] C. S. Fadley, X-ray photoelectron spectroscopy and diffraction in the hard x-ray regime: Fundamental considerations and future possibilities, *Nucl. Instrum. Methods Phys. Res., Sect. A* **547**, 24 (2005).
- [30] D. Payne, G. Paolicelli, F. Offi, G. Panaccione, P. Lacovig, G. Beamson, A. Fondacaro, G. Monaco, G. Vanko, and R. Egdell, A study of core and valence levels in β -PbO₂ by hard x-ray photoemission, *J. Electron Spectros. Relat. Phenomena* **169**, 26 (2009).
- [31] R. Claessen, M. Sing, M. Paul, G. Berner, A. Wetscherek, A. Müller, and W. Drube, Hard x-ray photoelectron spectroscopy of oxide hybrid and heterostructures: A new method for the study of buried interfaces, *New J. Phys.* **11**, 125007 (2009).
- [32] J. J. Mudd, T.-L. Lee, V. Muñoz Sanjosé, J. Zúñiga Pérez, D. J. Payne, R. G. Egdell, and C. F. McConville, Valence-band orbital character of CdO: A synchrotron-radiation photoelectron spectroscopy and density functional theory study, *Phys. Rev. B* **89**, 165305 (2014).
- [33] J. Woicik, ed., *Hard X-Ray Photoelectron Spectroscopy (HAXPES)*, Springer Series in Surface Sciences (Springer International Publishing, Cham, Switzerland, 2016), Vol. 59.
- [34] C. Kalha, N. K. Fernando, P. Bhatt, F. O. L. Johansson, A. Lindblad, H. Rensmo, L. Z. Medina, R. Lindblad, S. Siol, L. P. H. Jeurgens, C. Cancellieri, K. Rosnagel, K. Medjanik, G. Schönhense, M. Simon, A. X. Gray, S. Nemšák, P. Lömker, C. Schlueter, and A. Regoutz, Hard x-ray photoelectron spectroscopy: A snapshot of the state-of-the-art in 2020, *J. Phys.: Condens. Matter* **33**, 233001 (2021).
- [35] R. Griessen and A. Driessen, Heat of formation and band structure of binary and ternary metal hydrides, *Phys. Rev. B* **30**, 4372 (1984).
- [36] C. Schlueter, A. Gloskovskii, K. Ederer, I. Schostak, S. Piec, I. Sarkar, Y. Matveyev, P. Lömker, M. Sing, R. Claessen, C. Wiemann, C. M. Schneider, K. Medjanik, G. Schönhense, P. Amann, A. Nilsson, and W. Drube, The new dedicated HAXPES Beamline P22 at PETRAIII, AIP Conference Proceedings **2054** (2019).
- [37] See the Supplemental Material at <http://link.aps.org/supplemental/10.1103/PRXEnergy.3.013003> for the collected survey spectra, details on the peak-fitting procedure and DDF methodology, information on the resolution of the measurements, additional core-level and VB spectra, spectra collected after air exposure, the unweighted PDOS of both the metals and dihydrides, the complete cross-section-weighted dihydride PDOS at both 3.3- and 7.2-keV photon energies, additional computational details, a summary of the methods used to derive the enthalpy of formation from theory and experiment, and the HAXPES-collected Ti and Y metal VB spectra.
- [38] P. Hohenberg and W. Kohn, Inhomogeneous electron gas, *Phys. Rev.* **136**, 864 (1964).
- [39] W. Kohn and L. J. Sham, Self-consistent equations including exchange and correlation effects, *Phys. Rev.* **140**, 1133 (1965).
- [40] S. J. Clark, M. D. Segall, C. J. Pickard II, P. J. Hasnip, M. I. J. Probert, K. Refson, and M. C. Payne, First principles methods using CASTEP, *Z. Kristallogr.—Cryst. Materials* **220**, 567 (2005).
- [41] J. P. Perdew, K. Burke, and M. Ernzerhof, Generalized gradient approximation made simple, *Phys. Rev. Lett.* **77**, 3865 (1996).
- [42] H. J. Monkhorst and J. D. Pack, Special points for Brillouin-zone integrations, *Phys. Rev. B* **13**, 5188 (1976).
- [43] C. Adamo and V. Barone, Toward reliable density functional methods without adjustable parameters: The PBE0 model, *J. Chem. Phys.* **110**, 6158 (1999).
- [44] R. S. Mulliken, Electronic population analysis on LCAO-MO molecular wave functions. I, *J. Chem. Phys.* **23**, 1833 (1955).
- [45] M. D. Segall, R. Shah, C. J. Pickard, and M. C. Payne, Population analysis of plane-wave electronic structure calculations of bulk materials, *Phys. Rev. B* **54**, 16317 (1996).
- [46] M. D. Segall, C. J. Pickard, R. Shah, and M. C. Payne, Population analysis in plane wave electronic structure calculations, *Mol. Phys.* **89**, 571 (1996).
- [47] F. L. Hirshfeld, Bonded-atom fragments for describing molecular charge densities, *Theor. Chim. Acta* **44**, 129 (1977).
- [48] R. F. W. Bader, *Atoms in Molecules* (Oxford University Press, New York, 1990).
- [49] A. Arnaldsson, W. Tang, S. Chill, W. Chai, R. Anselm, and G. Henkelman, Bader charge analysis code (2022).
- [50] A. J. Morris, R. J. Nicholls, C. J. Pickard, and J. R. Yates, OptaDOS: A tool for obtaining density of states, core-level and optical spectra from electronic structure codes, *Comput. Phys. Commun.* **185**, 1477 (2014).
- [51] J. H. Scofield, *Theoretical Photoionization Cross Sections from 1 to 1500 keV*, Tech. Rep. (Lawrence Livermore Laboratory, 1973).
- [52] C. Kalha, N. Fernando, and A. Regoutz, Digitisation of Scofield photoionisation cross section tabulated data (2020), 10.6084/m9.figshare.12967079.v1.
- [53] A. J. Jackson, A. M. Ganose, A. Regoutz, R. G. Egdell, and D. O. Scanlon, GALORE: Broadening and weighting for simulation of photoelectron spectroscopy, *J. Open Source Software* **3**, 773 (2018).
- [54] A. Regoutz, Ph.D. thesis, Inorganic Chemistry Laboratory, University of Oxford, United Kingdom, 2016.
- [55] S. Tanuma, C. J. Powell, and D. R. Penn, Calculations of electron inelastic mean free paths. IX. Data for 41 elemental solids over the 50 eV to 30 keV range, *Surf. Interface Anal.* **43**, 689 (2011).
- [56] B. Lamartine, T. Haas, and J. Solomon, Characterization of TiH_x and TiD_{0.9} surfaces: AES, ELS, SIMS and XPS studies, *Appl. Surf. Sci.* **4**, 537 (1980).
- [57] L.-P. Ma, X.-D. Kang, H.-B. Dai, Y. Liang, Z.-Z. Fang, P.-J. Wang, P. Wang, and H.-M. Cheng, Superior catalytic effect of TiF₃ over TiCl₃ in improving the hydrogen

- sorption kinetics of MgH₂: Catalytic role of fluorine anion, *Acta Mater.* **57**, 2250 (2009).
- [58] N. Ren, G. Wang, H. Liu, and T. Ohachi, *In situ* synthesis of TiH₂ layer on metallic titanium foil through gaseous hydrogen free acid-hydrothermal method, *Mater. Res. Bull.* **50**, 379 (2014).
- [59] B. Biwer and S. Bernasek, A photoelectron and energy-loss spectroscopy study of Ti and its interaction with H₂, O₂, N₂ and NH₃, *Surf. Sci.* **167**, 207 (1986).
- [60] C. Sleigh, A. Pijpers, A. Jaspers, B. Coussens, and R. J. Meier, On the determination of atomic charge via ESCA including application to organometallics, *J. Electron Spectros. Relat. Phenomena* **77**, 41 (1996).
- [61] C. Fadley, Basic concepts of XPS, *Electron Spectrosc.: Theory, Tech. Appl.* **2**, 94 (1978).
- [62] S. Cornelius, G. Colombi, F. Nafezarefi, H. Schreuders, R. Heller, F. Munnik, and B. Dam, Oxyhydride nature of rare-earth-based photochromic thin films, *J. Phys. Chem. Lett.* **10**, 1342 (2019).
- [63] R. Reichl and K. Gaukler, An investigation of air-grown yttrium oxide and experimental determination of the sputtering yield and the inelastic mean free path, *Appl. Surf. Sci.* **26**, 196 (1986).
- [64] D. Barreca, G. A. Battiston, D. Berto, R. Gerbasi, and E. Tondello, Y₂O₃ thin films characterized by XPS, *Surf. Sci. Spectra* **8**, 234 (2001).
- [65] T. Gougousi and Z. Chen, Deposition of yttrium oxide thin films in supercritical carbon dioxide, *Thin Solid Films* **516**, 6197 (2008).
- [66] I. Z. Mitrovic, M. Althobaiti, A. D. Weerakkody, V. R. Dhanak, W. M. Linhart, T. D. Veal, N. Sedghi, S. Hall, P. R. Chalker, D. Tsoutsou, and A. Dimoulas, Ge interface engineering using ultra-thin La₂O₃ and Y₂O₃ films: A study into the effect of deposition temperature, *J. Appl. Phys.* **115**, 114102 (2014).
- [67] J. Pouilleau, D. Devilliers, F. Garrido, S. Durand-Vidal, and E. Mahé, Structure and composition of passive titanium oxide films, *Mater. Sci. Eng.: B* **47**, 235 (1997).
- [68] U. Diebold, The surface science of titanium dioxide, *Surf. Sci. Rep.* **48**, 53 (2003).
- [69] L. Huang, F. Peng, and F. S. Ohuchi, “*In situ*” XPS study of band structures at Cu₂O/TiO₂ heterojunctions interface, *Surf. Sci.* **603**, 2825 (2009).
- [70] J. Berens, S. Bichelmaier, N. K. Fernando, P. K. Thakur, T.-L. Lee, M. Mascheck, T. Wiell, S. K. Eriksson, J. M. Kahk, J. Lischner, M. V. Mistry, T. Aichinger, G. Pobegen, and A. Regoutz, Effects of nitridation on SiC/SiO₂ structures studied by hard x-ray photoelectron spectroscopy, *J. Phys.: Energy* **2**, 035001 (2020).
- [71] H. Shinotsuka, S. Tanuma, C. J. Powell, and D. R. Penn, Calculations of electron inelastic mean free paths. X. Data for 41 elemental solids over the 50 eV to 200 keV range with the relativistic full Penn algorithm, *Surf. Interface Anal.* **47**, 871 (2015).
- [72] A. Bosseboeuf, S. Lemetere, M. Wu, J. Moulin, P. Coste, C. Bessouet, S. Hammami, C. Renard, and L. Vincent, Effect of environment on activation and sorption of getter alloys and multilayers for hybrid wafer-level vacuum packaging, *Sens. Mater.* **31**, 2825 (2019).
- [73] C. Bessouet, S. Lemetere, C. Kutyla, A. Bosseboeuf, P. Coste, T. Sauvage, H. Lecoq, O. Wendling, A. Bellamy, P. Jagtap, S. Escoubas, C. Guichet, O. Thomas, and J. Moulin, Electrical and ion beam analyses of yttrium and yttrium-titanium getter thin films oxidation, *J. Vac. Sci. Technol. B* **39**, 054202 (2021).
- [74] F. Offi, K. Yamauchi, S. Picozzi, V. Lollobrigida, A. Verna, C. Schlueter, T.-L. Lee, A. Regoutz, D. Payne, A. Petrov, G. Vinai, G. Pierantozzi, T. Pincelli, G. Panaccione, and F. Borgatti, Identification of hidden orbital contributions in the La_{0.65}Sr_{0.35}MnO₃ valence band, *Phys. Rev. Materials* **5**, 104403 (2021).
- [75] S. Zhang and R. Xiao, Yttrium oxide films prepared by pulsed laser deposition, *J. Appl. Phys.* **83**, 3842 (1998).
- [76] S. Tanuma, C. J. Powell, and D. R. Penn, Calculation of electron inelastic mean free paths (IMFPs) VII. Reliability of the TPP-2M IMFP predictive equation, *Surf. Interface Anal.* **35**, 268 (2003).
- [77] W. C. Wang, M. Badylevich, V. V. Afanas’ev, A. Stesmans, C. Adelman, S. Van Elshocht, J. A. Kittl, M. Lukosius, C. Walczyk, and C. Wenger, Band alignment and electron traps in Y₂O₃ layers on (100)Si, *Appl. Phys. Lett.* **95**, 132903 (2009).
- [78] V. Mudavakkat, V. Atuchin, V. Kruchinin, A. Kayani, and C. Ramana, Structure, morphology and optical properties of nanocrystalline yttrium oxide (Y₂O₃) thin films, *Opt. Mater. (Amst)* **34**, 893 (2012).
- [79] J. Weaver and D. Peterson, Electronic structure studies of metal hydrides, *J. Less Common Metals* **74**, 207 (1980).
- [80] S. D. Barrett and R. G. Jordan, Angle-resolved UV photoemission from Y(0001), *Z. Phys. B Condens. Matter* **66**, 375 (1987).
- [81] R. Baptist, A. Pellissier, and G. Chauvet, On the origin of additional peaks in the photoelectron spectra of yttrium, *Z. Phys. B Condens. Matter* **73**, 107 (1988).
- [82] M. Budke, J. S. Correa, and M. Donath, Surface electronic structure of Y(0001): A consistent picture, *Phys. Rev. B* **77**, 161401 (2008).
- [83] D. O. Scanlon, C. W. Dunnill, J. Buckeridge, S. A. Shevlin, A. J. Logsdail, S. M. Woodley, C. R. A. Catlow, M. J. Powell, R. G. Palgrave, I. P. Parkin, G. W. Watson, T. W. Keal, P. Sherwood, A. Walsh, and A. A. Sokol, Band alignment of rutile and anatase TiO₂, *Nat. Mater.* **12**, 798 (2013).
- [84] S. Wendt, P. T. Sprunger, E. Lira, G. K. H. Madsen, Z. Li, J. O. Hansen, J. Matthesen, A. Blekinge-Rasmussen, E. Laegsgaard, B. Hamme, and F. Besenbacher, The role of interstitial sites in the Ti3d defect state in the band gap of titania, *Science* **320**, 1755 (2008).
- [85] C. M. Yim, C. L. Pang, and G. Thornton, Oxygen vacancy origin of the surface band-gap state of TiO₂(110), *Phys. Rev. Lett.* **104**, 036806 (2010).
- [86] C. Bigi, Z. Tang, G. M. Pierantozzi, P. Orgiani, P. K. Das, J. Fujii, I. Vobornik, T. Pincelli, A. Troglia, T.-L. Lee, R. Ciancio, G. Drazic, A. Verdini, A. Regoutz, P. D. C. King, D. Biswas, G. Rossi, G. Panaccione, and A. Selloni, Distinct behavior of localized and delocalized carriers in anatase TiO₂ (001) during reaction with O₂, *Phys. Rev. Materials* **4**, 025801 (2020).
- [87] M. Gupta, Electronically driven tetragonal distortion in TiH₂, *Solid State Commun.* **29**, 47 (1979).
- [88] H. Smithson, C. A. Marianetti, D. Morgan, A. Van der Ven, A. Predith, and G. Ceder, First-principles study of the

- stability and electronic structure of metal hydrides, *Phys. Rev. B* **66**, 144107 (2002).
- [89] D. J. Peterman, B. N. Harmon, J. Marchiando, and J. H. Weaver, Electronic structure of metal hydrides. II. Band theory of ScH₂ and YH₂, *Phys. Rev. B* **19**, 4867 (1979).
- [90] W. Wolf and P. Herzig, First-principles investigations of transition metal dihydrides, TH₂: T = Sc, Ti, V, Y, Zr, Nb; energetics and chemical bonding, *J. Phys.: Condens. Matter* **12**, 4535 (2000).
- [91] V. K. Mehta, S. C. Vogel, A. P. Shivprasad, E. P. Luther, D. A. Andersson, D. V. Rao, D. Kotlyar, B. Clausen, and M. W. Cooper, A density functional theory and neutron diffraction study of the ambient condition properties of sub-stoichiometric yttrium hydride, *J. Nucl. Mater.* **547**, 152837 (2021).
- [92] N. J. Luiggi A., Electronic, elastic, and topological behavior of MgH₂, MgTiH₄, and TiH₂ under pressure, *Materials Today Commun.* **28**, 102639 (2021).
- [93] R. Yang, Y. Wang, Y. Zhao, L. Wang, H. Ye, and C. Wang, Transition metal alloying effects on chemical bonding in TiH₂, *Acta Mater.* **50**, 109 (2002).
- [94] A. Allred, Electronegativity values from thermochemical data, *J. Inorg. Nucl. Chem.* **17**, 215 (1961).
- [95] M. Husain, A. Batra, and K. Srivastava, Electronegativity scale from x-ray photoelectron spectroscopic data, *Polyhedron* **8**, 1233 (1989).
- [96] K. Young, in *Reference Module in Chemistry, Molecular Sciences and Chemical Engineering* (Elsevier, Rochester hills, 2018).
- [97] K. H. J. Buschow, P. C. P. Bouten, and A. R. Miedema, Hydrides formed from intermetallic compounds of two transition metals: A special class of ternary alloys, *Rep. Prog. Phys.* **45**, 937 (1982).
- [98] A. Chernikov, V. Savin, V. Fadeev, N. Landin, and L. Izhevov, Thermodynamic and physical properties of yttrium and some rare earth hydrides, *J. Less Common Metals* **130**, 441 (1987).
- [99] E. M. Gray, Alloy selection for multistage metal-hydride hydrogen compressors: A thermodynamic model, *Int. J. Hydrogen Energy* **46**, 15702 (2021).
- [100] E. Huston and G. Sandrock, Engineering properties of metal hydrides, *J. Less Common Metals* **74**, 435 (1980).
- [101] P. Dantzer, High temperature thermodynamics of H₂ and D₂ in titanium, and in dilute titanium oxygen solid solutions, *J. Phys. Chem. Solids* **44**, 913 (1983).
- [102] J. wei Zhao, H. Ding, X. feng Tian, W. juan Zhao, and H. liang Hou, Thermodynamic calculation on the formation of titanium hydride, *Chin. J. Chem. Phys.* **21**, 569 (2008).
- [103] K. Miwa and A. Fukumoto, First-principles study on 3d transition-metal dihydrides, *Phys. Rev. B* **65**, 155114 (2002).
- [104] C. Wolverton, V. Ozoliņš, and M. Asta, Hydrogen in aluminum: First-principles calculations of structure and thermodynamics, *Phys. Rev. B* **69**, 144109 (2004).
- [105] S. X. Tao, P. H. L. Notten, R. A. van Santen, and A. P. J. Jansen, Density functional theory studies of the hydrogenation properties of Mg and Ti, *Phys. Rev. B* **79**, 144121 (2009).
- [106] H. Ziani and A. Gueddim, in *2020 6th International Symposium on New and Renewable Energy (SIENR)* (IEEE, Algeria, 2021), p. 1.
- [107] L. Ley, O. B. Dabbousi, S. P. Kowalczyk, F. R. McFeely, and D. A. Shirley, X-ray photoemission spectra of the valence bands of the 3d transition metals, Sc to Fe, *Phys. Rev. B* **16**, 5372 (1977).
- [108] H. Höchst, P. Steiner, G. Reiter, and S. Hüfner, XPS valence bands of Ti, Zr, Nb, Mo and Hf, *Z. Phys. B Condens. Matter* **42**, 199 (1981).
- [109] P. Blaha, K. Schwarz, and P. H. Dederichs, Electronic structure of hcp metals, *Phys. Rev. B* **38**, 9368 (1988).
- [110] K. Tanaka, M. Ushida, K. Sumiyama, and Y. Nakamura, Xps studies on the electronic structures of sputter-deposited and hydrogenated Ti-Pd alloy films, *J. Non. Cryst. Solids* **117-118**, 429 (1990).